Estimation of P-S-N curves in very-high-cycle fatigue: Statistical procedure based on a general crack growth rate model

(Article begins on next page)

17 April 2024

Estimation of P-S-N curves in Very-High-Cycle Fatigue: statistical procedure based on a general crack growth rate model

Authors:

D.S. Paolino[a], A. Tridello[b], G. Chiandussi[c], M. Rossetto[d]

[a] Department of Mechanical and Aerospace Engineering, Politecnico di Torino, 10129 Turin, Italy, davide.paolino@polito.it

[b] Department of Mechanical and Aerospace Engineering, Politecnico di Torino, 10129 Turin, Italy, andrea.tridello@polito.it

[c] Department of Mechanical and Aerospace Engineering, Politecnico di Torino, 10129 Turin, Italy, giorgio.chiandussi@polito.it

[d] Department of Mechanical and Aerospace Engineering, Politecnico di Torino, 10129 Turin, Italy, massimo.rossetto@polito.it

Corresponding Author:

D.S. Paolino

E-mail address: davide.paolino@polito.it

Full postal address:

C.so Duca degli Abruzzi 24,

Department of Mechanical and Aerospace Engineering – Politecnico di Torino,

10129 – Turin,

ITALY

Phone number: +39.011.090.5746

Fax number: +39.011.090.6999

Abstract:

Extensive experimental investigations show that internal defects play a key role in the Very-High-Cycle Fatigue (VHCF) response of metallic materials and that crack growth from internal defects can take place even if the Stress Intensity Factor (SIF) associated to the initial defect is below the threshold for crack growth. By introducing a reduction term in the typical formulation of the threshold for crack growth, the Authors recently proposed a general phenomenological model, which can effectively describe crack growth from internal defects in VHCF. The model is able to consider the different crack growth scenarios that may arise in VHCF and is general enough to embrace the various weakening mechanisms proposed in the literature for explaining why crack can grow below the threshold.

In the present paper, the model is generalized in a statistical framework. The statistical distributions of the crack growth threshold and of the initial defect size are introduced in the model. The procedure for the estimation of the Probabilistic-S-N curves and of the fatigue limit distribution is illustrated and numerically applied to an experimental dataset.

Acronyms and nomenclature

FGA: Fine Granular Area

HV: Vickers Hardness

LEV: Largest Extreme Value

SIF: Stress Intensity Factor

$\sqrt{a}$, $\sqrt{a_0}$, $\sqrt{a_{FGA}}$: characteristic defect sizes, deterministic values

$\sqrt{a_0^*}$, $\sqrt{a_{FGA}^*}$, $\sqrt{a_{0,\infty}^*}$, $k_{th,g}^*$, $k_{th,l}^*$, $k_{th,r}^*$, n_f^*, z^*: random simulations

$\sqrt{A_0}$: initial defect size, random variable

c_{s_l}, $c_{th,g}$, $c_{th,r}$, $\alpha_{th,g}$, $\alpha_{th,r}$: constant coefficients in threshold SIFs and fatigue limit

c_I, m_I, c_{II}, m_{II}, c_{II}, m_{II}: Paris' constants

$f_{\sqrt{A_0}}$: probability density function of $\sqrt{A_0}$

$F_{\sqrt{A_0}}$, $F_{N_f,\sqrt{a_0}}$: cumulative distribution functions

k_d, $k_{th,g}$, $k_{th,l}$, $k_{th,r}$: characteristic SIFs, deterministic values

n_I, n_{II}, n_{III}, n_f: number of cycles, deterministic values

s: applied stress amplitude, deterministic value

s_l: fatigue limit, deterministic value

$\mu_{\sqrt{A}}$, $\sigma_{\sqrt{A}}$, $\sigma_{th,g}$: parameters of statistical distributions

$\sqrt{a_{FGA,\alpha}}$, $k_{th,g,\alpha}$, $n_{f,\sqrt{a_0},\alpha}$, $s_{l,\sqrt{a_0},\alpha}$, z_α: α-th quantiles

$\tilde{\ }$: parameter estimate

1. Introduction

Very-High-Cycle Fatigue (VHCF) is a quite recent and attractive research field related to the fatigue response of materials for number of cycles larger than 10^8. Extensive experimental investigations performed on several metallic materials show that VHCF failures mainly originate from internal or subsurface defects and typically exhibit fracture surfaces with the fish-eye morphology. Within the fish-eye, fracture surfaces also exhibit the so-called Fine Granular Area (FGA)[1] around the initial defect.

It is well-known[2-6] that the FGA plays a major role in the VHCF response, since more than the 95% of the total life is consumed in its formation. The average crack growth rate within the FGA is extremely small and, unexpectedly, crack can grow even if the Stress Intensity Factor (SIF) is smaller than the threshold value for crack growth. To explain such peculiarity, several micromechanical models are proposed in the VHCF literature: local grain refinement[2, 4-8], hydrogen embrittlement[3, 9, 10], carbide decohesion[11], matrix fragmentation[12] or formation of persistent slip bands[13]. The common aspect of each micromechanical model is that a weakening mechanism occurs around the initial defect, thus permitting crack growth below the SIF threshold.

In[14], the Authors proposed and experimentally validated a model for crack growth from an internal defect in the VHCF regime. In a subsequent paper[15], the Authors also showed that the model can be effectively used for a quantitative description of the different crack growth scenarios that may arise in VHCF and is general enough to embrace the various weakening mechanisms proposed in the literature.

In the present paper, the model is generalized in a statistical framework. The statistical distributions of the crack growth threshold and of the initial defect size are introduced in the model. The procedure for the estimation of the Probabilistic-S-N curves and of the fatigue limit distribution is illustrated and numerically applied to an experimental dataset.

2. Methods

In Section 2.1, a general expression for modeling the crack growth rate from the initial internal defect up to the VHCF failure is presented. In Section 2.2, the statistical distribution of the fatigue limit is analytically defined. Finally, Section 2.3 defines a procedure for the estimation of the Probabilistic-S-N (P-S-N) curves.

In the following, according to[15], k_d denotes the SIF at the internal defect, $k_{th,g}$ denotes the global SIF threshold, $k_{th,r}$ denotes the reduction SIF threshold, $k_{th,l}$ denotes the local SIF threshold (i.e., $k_{th,l} = k_{th,g} - k_{th,r}$), a_0 is the projected area of the initial defect and a_{FGA} is the projected area of the FGA.

2.1. Crack growth rate within the FGA

In the VHCF literature[6, 16-18], the crack growth rate within the FGA is commonly modeled with the Paris' law and the related crack growth rate diagram (Fig. 1) generally consists of three stages:

- Stage I: the below-threshold region within the FGA, from k_{a_0} (SIF associated to the initial defect) up to $k_{th,g}$;

- Stage II: the steady stage, from the border of the FGA (SIF equal to $k_{th,g}$) up to the border of the fish-eye (with SIF equal to k_{FiE});

- Stage III: the unsteady stage, beyond the fish-eye border (with SIF larger than k_{FiE}, up to the failure).
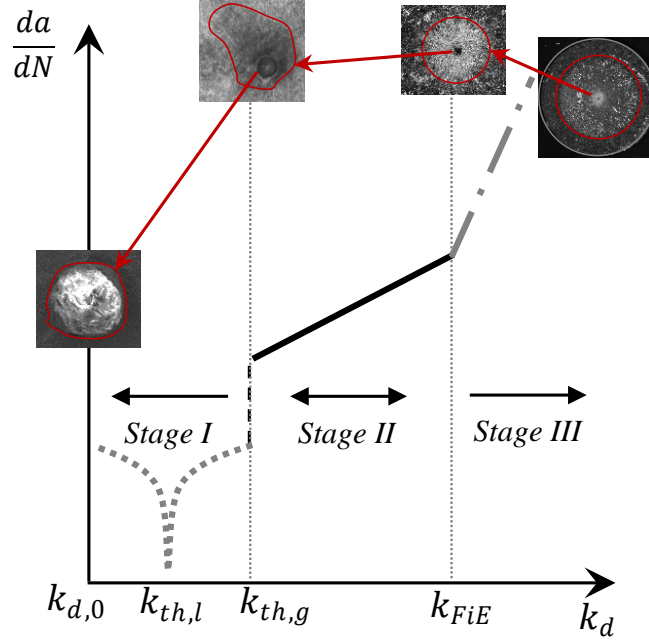
Figure 1: The three stages of crack propagation in a crack growth rate diagram for VHCF failures from internal defects.

The modified Paris' law proposed in[19] was considered for modeling the crack growth within the FGA:

$$\frac{da}{dN} = c_I\left(k_d - k_{th,l}\right)^{m_I},$$ (1)

where c_I and m_I are the Paris' constants related to Stage I, from the initial defect size $\sqrt{a_0}$ up to $\sqrt{a_{FGA}}$.

In Stage II, from the border of the FGA up to the border of the fish-eye, the crack growth rate was modeled with the conventional Paris' law[16-18]:

$$\frac{da}{dN} = c_{II} k_d^{m_{II}},$$ (2)

where c_{II} and m_{II} are the two Paris' constants related to Stage II, from $\sqrt{a_{FGA}}$ up to $\sqrt{a_{FiE}}$.

If crack propagation takes also place beyond the fish-eye border, a third stage is visible on fracture surfaces and it was modeled, again, with the conventional Paris' law[18]:

$$\frac{da}{dN} = c_{III} k_d^{m_{III}},$$ (3)

where c_{III} and m_{III} are the two Paris' constants related to Stage III, from $\sqrt{a_{FiE}}$ up to $\sqrt{a_c}$ at the border of the final fracture. It is worth to note that, it often occurs that the final fracture takes place when the crack size reaches the border of the fish-eye. In these cases, Stage III is not present.

The number of cycles to failure, n_f, is the sum of the number of cycles consumed within the three stages of propagation:

$$n_f = n_I + n_{II} + n_{III}.$$ (4)

Following the VHCF literature[6, 18, 20], n_I was estimated by subtracting, from the experimental n_f, the numbers of cycles consumed in Stages II and III, which, in turn, were obtained through integration of Eqs. (2) and (3), respectively.

According to[15], the experimental n_I values ($n_{I,exp}$) were used for the estimation of the Paris' constants c_I, m_I and of the parameters $c_{th,r}$ and $\alpha_{th,r}$ involved in the expression of $k_{th,l}$. Parameter estimates were obtained through the nonlinear Least Squares Method by minimizing the sum of squared percent errors between the experimental $\log_{10}(n_{I,exp})$ values and the estimated $\log_{10}(n_{I,est})$ values computed through integration of Eq. (1).

2.2. Fatigue limit expression and related statistical distribution

As reported in[14, 15], the fatigue limit, referred to as s_l, is given by:

$$s_l = c_{s_l} \frac{c_{th,g}(HV+120)}{\sqrt{a_0}^{1/2-\alpha_{th,g}}},$$ (5)

where $c_{s_l} = \left(\frac{(1/2-\alpha_{th,g})0.5\sqrt{\pi}}{(\alpha_{th,g}-\alpha_{th,r})c_{th,r}}\right)^{\frac{1/2-\alpha_{th,g}}{1/2-\alpha_{th,r}}} \frac{\alpha_{th,g}-\alpha_{th,r}}{0.5\sqrt{\pi}(1/2-\alpha_{th,r})}$ depends on the four coefficients, $c_{th,g}$, $\alpha_{th,g}$, $c_{th,r}$ and $\alpha_{th,r}$, involved in the expressions of the global SIF threshold $k_{th,g}$:

$$k_{th,g} = c_{th,g}(HV+120)\sqrt{a}^{-\alpha_{th,g}},$$ (6)

and of the reduction SIF threshold $k_{th,r}$:

$$k_{th,r} = c_{th,r}s\sqrt{a_0}^{-1/2}\left(\sqrt{a}/\sqrt{a_0}\right)^{\alpha_{th,r}},$$ (7)

being a is the projected area of the defect, a_0 the projected area of the initial defect, s the local stress amplitude at the defect location and HV the Vickers hardness of the material.

Eq. (5) recalls the well-known expression proposed by Murakami[9] and it is obtained by considering the condition of transition between finite and infinite fatigue life, for a given initial defect size (Fig. 2).
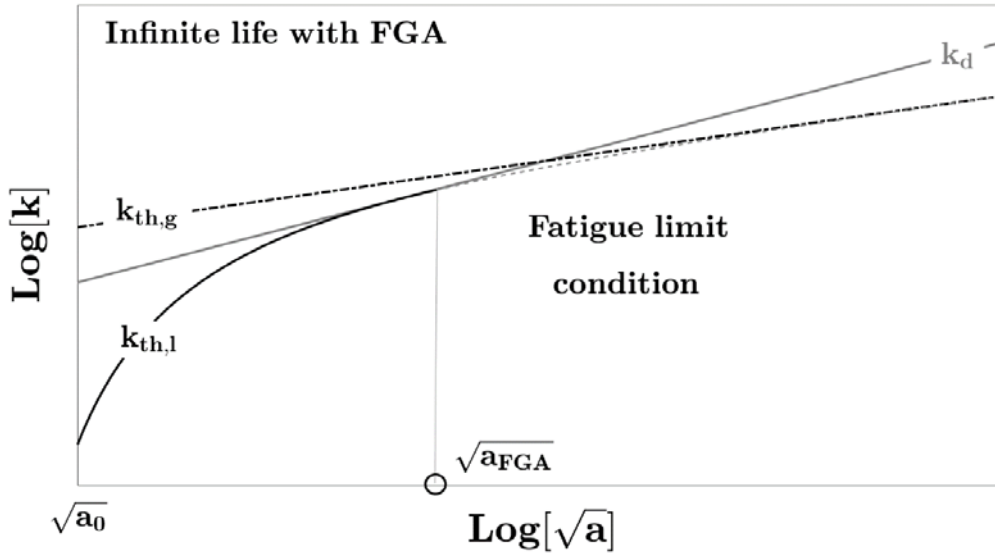

Figure 2: Variation of relevant SIFs with defect size in fatigue limit condition.

The statistical distribution of the fatigue limit for a given initial defect size (conditional distribution of the fatigue limit) is defined according to[14]:

$$s_{l,\sqrt{a_0},\alpha} = c_{s_l} \frac{c_{th,g}(HV+120)}{\sqrt{a_0}^{1/2-\alpha_{th,g}}} 10^{z_\alpha \sigma_{th,g}},$$ (8)

where $s_{l,\sqrt{a_0},\alpha}$ is the α-th quantile of the conditional distribution, z_α denotes the α-quantile of a standardized Normal distribution and $\sigma_{th,g}$ is the standard deviation of the global SIF threshold[14, 15].

Eq. (8) is obtained by assuming, according to the literature[14, 21, 22], a Lognormal distribution for the global SIF threshold:

$$k_{th,g,\alpha} = c_{th,g}(HV + 120)\sqrt{a}^{-\alpha_{th,g}}10^{z_\alpha\sigma_{th,g}}, \tag{9}$$

where $k_{th,g,\alpha}$ denotes the α-th quantile of the global SIF threshold.

2.3. Conditional and marginal P-S-N curves

The Probabilistic-S-N (P-S-N) curves model the random variation of the fatigue life for different stress amplitudes. Their identification was based on the integration of Eq. (1) and on the assumption that the number of cycles consumed in Stages II and III was negligible with respect to that spent within Stage I (i.e., $n_f \cong n_I$). It is worth to note that the assumption yielded quasi-correct n_f values since, according to the literature[5, 6, 15, 20], more than the 95% of the total VHCF life is generally spent in Stage I. In particular, in[15], it is shown that n_I/n_f is always larger than the 99.5%.

The integration of Eq. (1) permitted to estimate the α-th quantile of the fatigue life for a given initial defect size (conditional P-S-N curve):

$$n_{f,\sqrt{a_0},\alpha} \cong n_{I,\sqrt{a_0},\alpha} = \int_{\sqrt{a_0}}^{\sqrt{a_{FGA,\alpha}}} \frac{da}{c_I(k_d - k_{th,l,\alpha})^{m_I}}, \tag{10}$$

where $k_d = 0.5s\sqrt{\pi}\sqrt{a}^{1/2}$ is the SIF for an internal defect, $k_{th,l,\alpha} = k_{th,g,\alpha} - k_{th,r}$ denotes the α-th quantile of the local SIF threshold and $\sqrt{a_{FGA,\alpha}}$ is the α-th quantile of the FGA size:

$$\sqrt{a_{FGA,\alpha}} = \left(\frac{c_{th,g}(HV+120)10^{z_\alpha\sigma_{th,g}}}{0.5s\sqrt{\pi}}\right)^{\frac{1}{1/2-\alpha_{th,g}}}. \tag{11}$$

The expression in Eq. (11) was obtained by considering that, when the defect size reaches $\sqrt{a_{FGA,\alpha}}$, k_d is necessarily equal to $k_{th,g,\alpha}$.

The marginal distribution of the fatigue life, no more conditioned to the value assumed by $\sqrt{a_0}$, (marginal P-S-N curve) was identified by introducing the distribution of the initial defect size. Since the initial defect size is the size of the largest defect present in the specimen[9], the initial defect size random variable, referred to as $\sqrt{A_0}$, was modelled through a Type I Largest Extreme Value (LEV) distribution[9] with probability density function:

$$f_{\sqrt{A_0}}(\sqrt{a_0}) = \frac{e^{-\frac{\sqrt{a_0}-\mu_{\sqrt{A}}}{\sigma_{\sqrt{A}}}-e^{-\frac{\sqrt{a_0}-\mu_{\sqrt{A}}}{\sigma_{\sqrt{A}}}}}}{\sigma_{\sqrt{A}}}, \tag{12}$$

where $\mu_{\sqrt{A}}$ and $\sigma_{\sqrt{A}}$ are the two parameters of the LEV distribution and are easily estimated through a Gumbel plot of the initial defect sizes, according to the procedure suggested in[9].

The α-th quantile of the marginal distribution of the fatigue limit was obtained by taking into account the defect size distribution:

$$\alpha = \int_0^\infty F_{N_f,\sqrt{a_0}}(n_{f,\alpha}; s, \sqrt{a_0}) \cdot f_{\sqrt{A_0}}(\sqrt{a_0}) \cdot d\sqrt{a_0}, \tag{13}$$

where $F_{N_f, \sqrt{a_0}}$ denotes the conditional distribution of the fatigue life. Given $F_{N_f, \sqrt{a_0}}$, the α-th quantile of the fatigue life could be obtained by solving Eq. (13) with respect to $n_{f,\alpha}$ for different values of s.

$F_{N_f, \sqrt{a_0}}$ was implicitly defined in Eq. (10). However, the complexity of the expression of $n_{f, \sqrt{a_0}, \alpha}$ in Eq. (10) did not permit to define an explicit function for $F_{N_f, \sqrt{a_0}}$, which was necessary for computing $n_{f,\alpha}$ from Eq. (13). Therefore, $n_{f,\alpha}$ was not obtained from Eq. (13) and an alternative numerical procedure was adopted in substitution. The procedure was based on Montecarlo simulations of the number of cycles to failure for a given stress amplitude s. The following steps were followed for each Montecarlo simulation:

1) Definition of a stress amplitude value, s;
2) Random extraction of an initial defect size, $\sqrt{a_0^*}$, from the estimated $f_{\sqrt{A_0}}(\sqrt{a_0})$;
3) Random extraction of a value, z^*, from the standard Normal distribution;
4) Computation of a random global SIF threshold, $k_{th,g}^*$, from Eq. (9) with z_α replaced by z^*;
5) Computation of a random reduction SIF threshold, $k_{th,r}^*$, from Eq. (7) with $\sqrt{a_0}$ replaced by $\sqrt{a_0^*}$;
6) Computation of a random local SIF threshold, $k_{th,l}^* = k_{th,g}^* - k_{th,r}^*$;
7) Computation of a random FGA size, $\sqrt{a_{FGA}^*}$, from Eq. (11) with z_α replaced by z^*;
8) Computation of $\sqrt{a_{0,\infty}^*}$, the initial defect size yielding a fatigue limit equal to s:

$$\sqrt{a_{0,\infty}^*} = \left(c_{s_l} \frac{c_{th,g}(HV+120)}{s} 10^{z^* \sigma_{th,g}} \right)^{\frac{1}{1/2 - \alpha_{th,g}}};$$ (14)

9) Computation of a random number of cycles, n_f^*, at s:

$$n_f^* = \begin{cases} \infty, & \sqrt{a_0^*} \leq \sqrt{a_{0,\infty}^*} \\ \int_{\sqrt{a_0^*}}^{\sqrt{a_{FGA}^*}} \frac{da}{c_I (k_d - k_{th,l}^*)^{m_I}}, & \sqrt{a_{0,\infty}^*} < \sqrt{a_0^*} < \sqrt{a_{FGA}^*}; \\ 0, & \sqrt{a_0^*} \geq \sqrt{a_{FGA}^*} \end{cases}$$ (15)

Steps 1) to 9) were repeated 10000 times to permit an accurate estimation of the marginal distribution of the number of cycles to failure. It is worth to note that the case $\sqrt{a_0^*} \geq \sqrt{a_{FGA}^*}$ in step 9) is a very rare condition in the VHCF regime. Indeed, the random FGA size $\sqrt{a_{FGA}^*}$ reduces for larger stress amplitudes and it may reach values smaller than $\sqrt{a_0^*}$ only for stress amplitudes in the High-Cycle Fatigue (HCF) regime. Since the analysis was performed for studying the VHCF regime, the condition $\sqrt{a_0^*} \geq \sqrt{a_{FGA}^*}$ did not occur in almost all Montecarlo simulations.

The distribution of the number of cycles to failure at s was then estimated with the Kaplan-Meier estimator[23] from the simulated 10000 fatigue lives. Finally, the α-th quantile of the fatigue life, $n_{f,\alpha}$, was easily computed from the estimated distribution. The procedure was repeated for several stress amplitudes in the VHCF region, in order to estimate the marginal P-S-N curves.

3. Numerical application to an experimental dataset

In order to show the applicability of the proposed approach, model parameters were fitted to an experimental dataset.

VHCF tests were carried out on Gaussian specimens[24] made of an AISI H13 steel with Vickers hardness 560 kg$_f$/mm^2. Details on the testing setup and on the tested material are reported in[25, 26] and will not be recalled here for the sake of brevity. Twelve specimens were loaded at a constant stress amplitude up to failure. The number of cycles to failure ranged from 4.2×10^7 to 3.85×10^9. Fracture surfaces were seen through a Scanning-Electron-Microscope (SEM) in order to measure the initial defect size (i.e., $\sqrt{a_0}$) in each specimen;

whereas, the FGA sizes (i.e., $\sqrt{a_{FGA}}$) were measured from pictures taken at the optical microscope. From the SEM analysis, all the fatigue fractures nucleated from non-metallic inclusions (oxide-type inclusions).

The local stress amplitude in the vicinity of the initial defect was considered as the stress amplitude applied during the test. As shown in the S-N plot of the experimental dataset (Fig. 3), the local stress amplitudes were in the range 500–635 MPa.
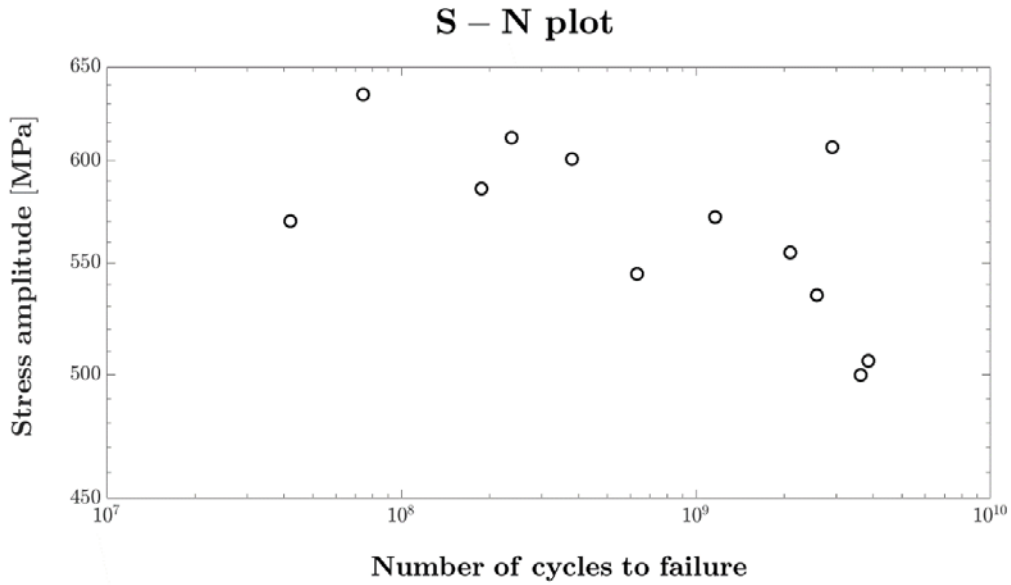

Figure 3: S-N plot of the experimental dataset.

The parameters $c_{th,g}$, $\alpha_{th,g}$ and $\sigma_{th,g}$ involved in the expressions of the α-th quantile of the fatigue limit (Eq. 8) and of the global SIF threshold (Eq. 9) were estimated following the procedure described in[15]. Fig. 4 shows the $k_{th,g}$ values with respect to $\sqrt{a_{FGA}}$, together with the estimated model. The 0.1-th and the 0.9-th quantiles are also depicted.
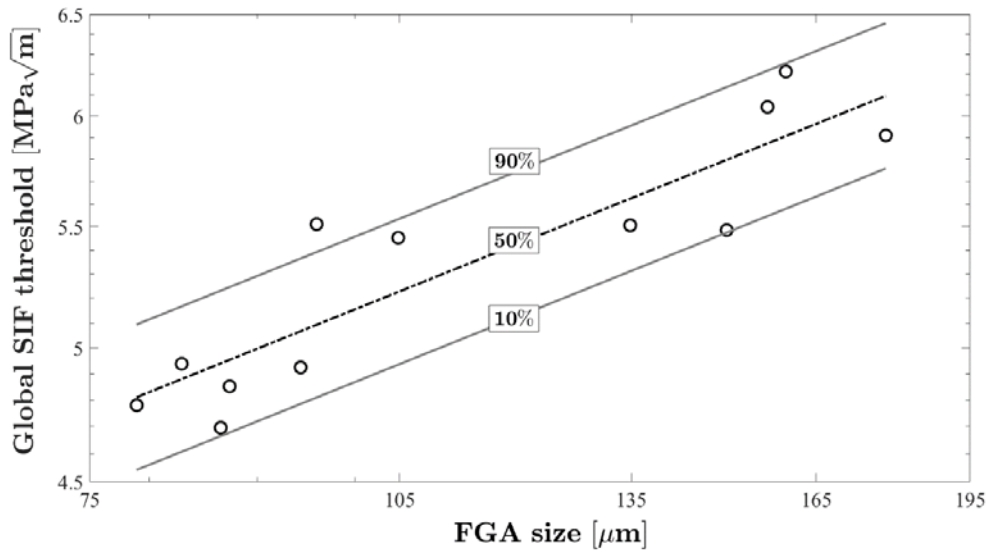

Figure 4: Global SIF threshold variation as a function of the FGA size.

In particular, the following estimates of $c_{th,g}$, $\alpha_{th,g}$ and $\sigma_{th,g}$ were obtained:

$$\begin{cases} \widetilde{c_{th,g}} = 1.979 \cdot 10^{-3} \\ \widetilde{\alpha_{th,g}} = 0.2916 \\ \widetilde{\sigma_{th,g}} = 0.0194 \end{cases} , \qquad\qquad\qquad (16)$$

where $\widetilde{}$ denotes the parameter estimate. It is worth noting that the estimates $\widetilde{c_{th,g}}$ and $\widetilde{\alpha_{th,g}}$ are in agreement with the values proposed in the literature for $c_{th,g}$[27, 28] and for $\alpha_{th,g}$[3, 9, 27, 28]. As shown in Fig. 4, the assumed linear model is in good agreement with the experimental data (11 failures out of 12 are inside the 80% confidence interval).

The parameters c_I, m_I, $c_{th,r}$ and $\alpha_{th,r}$ were estimated through the nonlinear Least Squares Method[15], which yielded the following estimates:

$$\begin{cases} \widetilde{c_I} = 2.2832 \times 10^{-15} \\ \widetilde{m_I} = 4.0522 \\ \widetilde{c_{th,r}} = 0.9150 \\ \widetilde{\alpha_{th,r}} = -0.0926 \end{cases} . \qquad\qquad\qquad (17)$$

The fatigue limit for a given defect size was then estimated according to Eq. (8). Fig. 5 shows the median, the 0.1-th and the 0.9-th quantiles of fatigue limit as a function of the initial defect size.
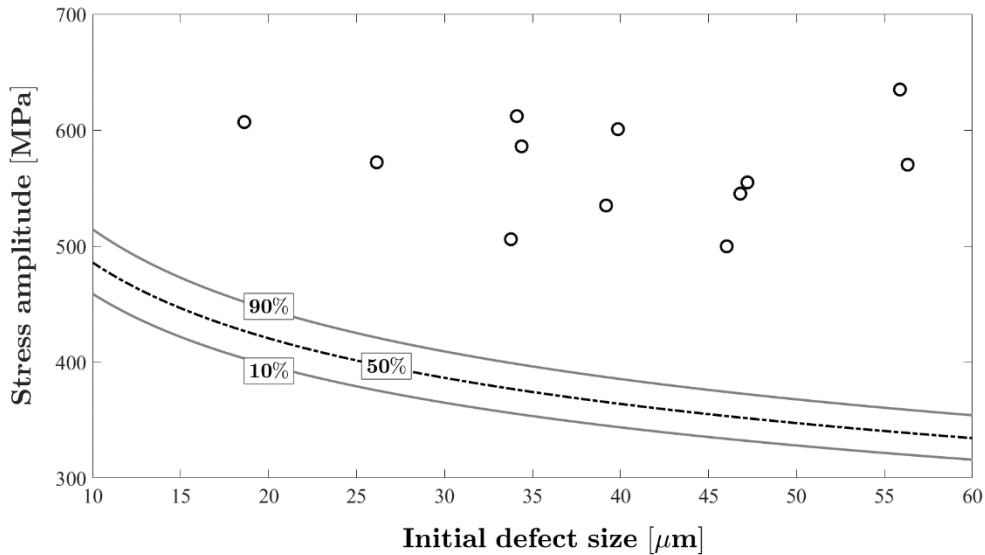

Figure 5: Variation of the fatigue limit with the initial defect size.

Fig. 5 shows, in agreement with the literature[9, 29], that the fatigue limit decreases with the initial defect size. The estimated fatigue limit curves are below the experimental failures, as expected from the definition of fatigue limit. The proposed model was therefore effective in the estimation of the fatigue limit variation with respect to the initial defect size and ensured a reliable safety margin with respect to the experimental failures.

Conditional P-S-N curves were estimated for all the initial defect sizes in the experimental dataset, according to Eq. (10). Fig. 6 depicts the estimated curves, which confirm the appropriateness of the proposed model: except for one case ($\sqrt{a_0}$ = 46.2 µm), experimental data are within the plotted curves that, according to the literature[9], move downward (to smaller VHCF strength values) and leftward (to smaller VHCF life) if the initial defect size increases. Moreover, the trend followed by the curves in the finite VHCF region (from 10^8 to 10^{10} cycles) is in good agreement with the Basquin's model (linear trend in a bi-logarithmic S-N plot), which is commonly assumed for fitting VHCF data[27, 30, 31].
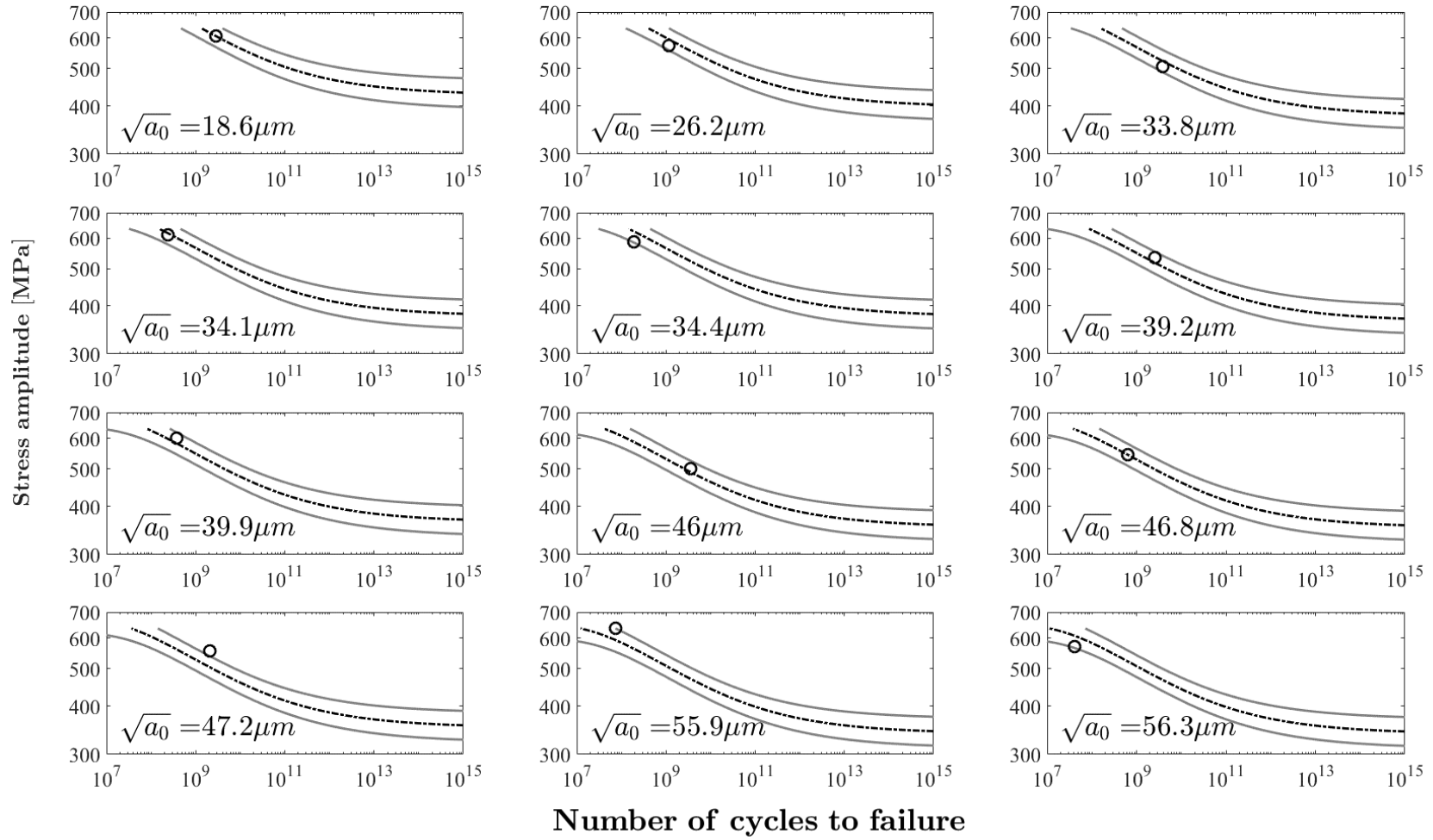
Figure 6: Conditional P-S-N curves estimated for the initial defect sizes of the experimental dataset. The three curves in each graph correspond to the 0.025-th, 0.5-th and 0.975-th quantiles of the VHCF life.

The distribution of initial defect size was estimated according to[9]. Fig. 7 shows the Gumbel plot of the initial defect size together with the estimated LEV distribution ($\widetilde{\mu_{\sqrt{A}}} = 34.35$ µm and $\widetilde{\sigma_{\sqrt{A}}} = 10.73$ µm).
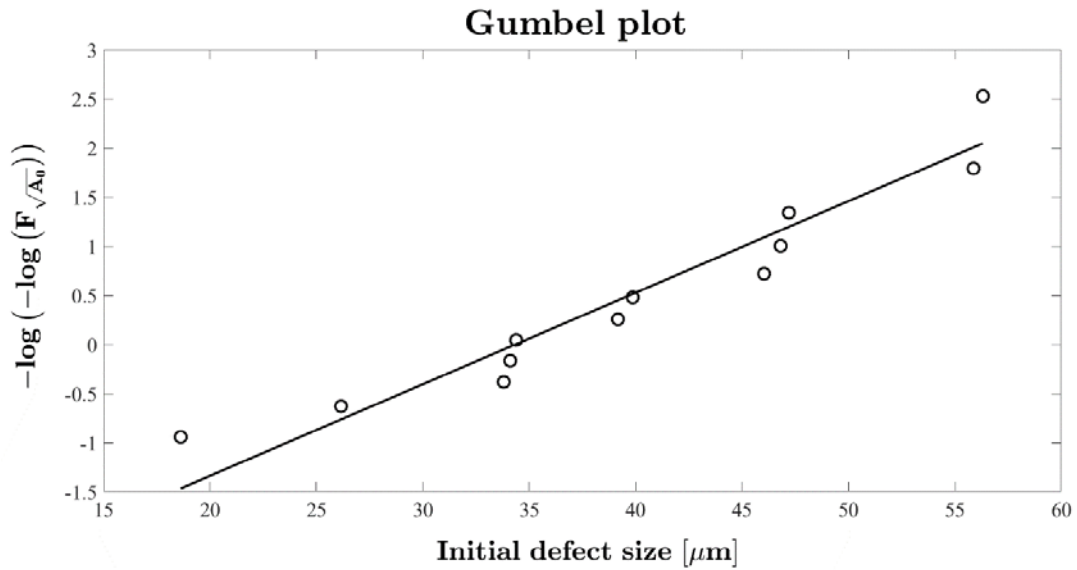
Figure 7: Gumbel plot of the initial defect size for the investigated steel.

Marginal P-S-N curves were finally estimated through Montecarlo simulations, according to the procedure described in Section 2.3. Fig. 8 shows the estimated curves together with the experimental data in a bi-logarithmic S-N plot.
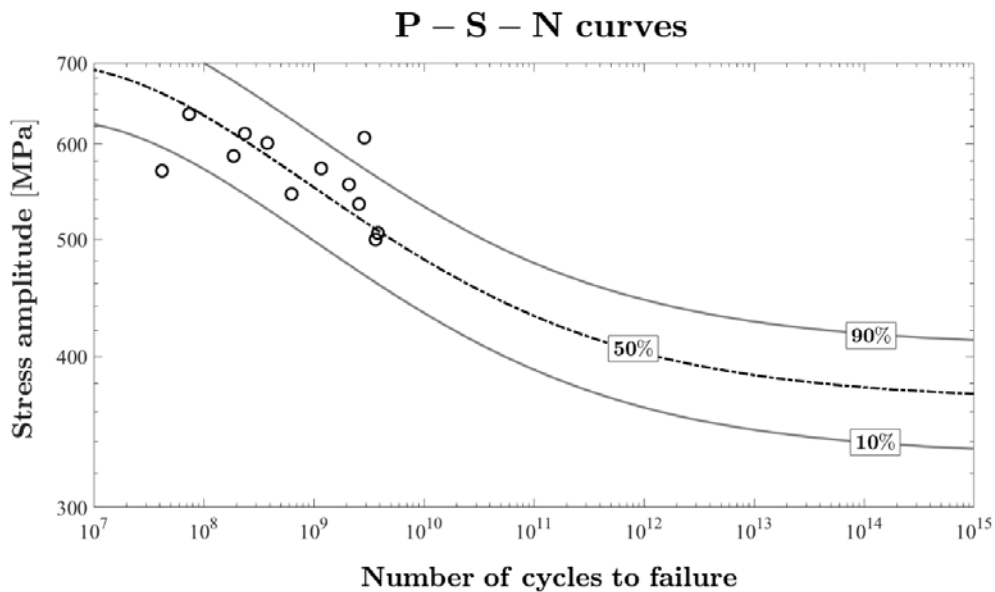

Figure 8: Marginal P-S-N curves for the experimental dataset.

As shown in Fig. 8, the estimated P-S-N curves exhibit a sigmoidal trend and well fit the experimental data: the 83% of data (ten out of twelve failures) is within the 10% and the 90% P-S-N curves and the 50% of data (six out of twelve failures) is below the median P-S-N curve. In the finite VHCF region (from 10^8 to 10^{10} cycles), the curves follow a trend in good agreement with the Basquin's model[27, 30, 31]. For number of cycles smaller than 10^7 and larger than 10^{12}, the curves approach two horizontal plateaux, which correspond to the transition stress between HCF and VHCF and to the VHCF limit.

4. Conclusions

In the present paper, the procedure for the estimation of the P-S-N curves was discussed and successfully applied to an experimental dataset.

The procedure introduced, in a general crack growth rate model recently proposed by the Authors, the statistical distributions of the crack growth threshold and of the initial defect size.

Two kinds of P-S-N curves were estimated: conditional P-S-N curves, if curves are for a given initial defect size, and marginal P-S-N curves, if curves are regardless of the initial defect size. The estimation of the conditional P-S-N curves was based on the direct integration of the modified Paris' law adopted to model the first stage of crack growth, from the initial defect to the FGA border. Due to the complexity of the analytical expression, the marginal P-S-N curves were estimated following a numerical approach based on Montecarlo simulations.

The procedure proved effective when applied to an experimental dataset. Conditional and marginal P-S-N curves were in good agreement with the experimental data and showed a sigmoidal trend consisting of three distinct regions in a bi-logarithmic S-N plot:

- An upper horizontal plateau corresponding to the transition from HCF to VHCF, for number of cycles smaller than 10^7;
- A central linear trend corresponding to the finite VHCF, for number of cycles from 10^8 to 10^{10} cycles;
- A lower horizontal plateau corresponding to the VHCF limit, for number of cycles larger than 10^{12}.

The numerical application showed the potentialities of the proposed approach in terms of estimated statistical results (conditional and marginal P-S-N curves) and it also highlighted the ease of application of the method.

References

1. Sakai T, Sato Y, Oguma N (2002) Characteristics S-N properties of high-carbon-chromium-bearing steel under axial loading in long-life fatigue. *Fatigue and Fracture of Engineering Materials and Structures*. **25**: 765-773.
2. Grad P, Reuscher B, Brodyanski A, Kopnarski M, Kerscher E (2012) Mechanism of fatigue crack initiation and propagation in the very high cycle fatigue regime of high-strength steels. *Scripta Materialia*. **67**: 838-841.
3. Matsunaga H, Sun C, Hong Y, Murakami Y (2015) Dominant factors for very-high-cycle fatigue of high-strength steels and a new design method for components. *Fatigue & Fracture of Engineering Materials & Structures*. **38**: 1274-1284.
4. Sakai T, Oguma N, Morikawa A (2015) Microscopic and nanoscopic observations of metallurgical structures around inclusions at interior crack initiation site for a bearing steel in very high-cycle fatigue. *Fatigue & Fracture of Engineering Materials & Structures*. **38**: 1305-1314.
5. Hong Y, Liu X, Lei Z, Sun C (2016) The formation mechanism of characteristic region at crack initiation for very-high-cycle fatigue of high-strength steels. *International Journal of Fatigue*. **89**: 108-118.
6. Hong Y, Sun C (In press) The nature and the mechanism of crack initiation and early growth for very-high-cycle fatigue of metallic materials – An overview. *Theoretical and Applied Fracture Mechanics*.
7. Sakai T (2009) Review and prospects for current studies on very high cycle fatigue of metallic materials for machine structural use. *Journal of solid mechanics and materials engineering*. **3**: 425-439.
8. Nakamura T, Oguma H, Shinohara Y (2010) The effect of vacuum-like environment inside sub-surface fatigue crack on the formation of ODA fracture surface in high strength steel. *Fatigue 2010*. **2**: 2121-2129.
9. Murakami Y (2002) *Metal Fatigue: Effects of Small Defects and Non-Metallic Inclusions*. Elsevier, Oxford, UK.
10. Liu YB, Li YD, Li SX, et al. (2010) Prediction of the S-N curves of high-strength steels in the very high cycle fatigue regime. *International Journal of Fatigue*. **32**: 1351-1357.
11. Shiozawa K, Lu L, Ishihara S (2001) S-N curve characteristics and subsurface crack initiation behaviour in ultra-long life fatigue of a high carbon-chromium bearing steel. *Fatigue and Fracture of Engineering Materials and Structures*. **24**: 781-790.
12. Shanyavskiy AA (2013) Mechanisms and modeling of subsurface fatigue cracking in metals. *Engineering Fracture Mechanics*. **110**: 350-363.
13. Huang Z, Wagner D, Bathias C, Paris PC (2010) Subsurface crack initiation and propagation mechanisms in gigacycle fatigue. *Acta Materialia*. **58**: 6046-6054.
14. Paolino DS, Tridello A, Chiandussi G, Rossetto M (2016) S-N curves in the very-high-cycle fatigue regime: statistical modeling based on the hydrogen embrittlement consideration. *Fatigue & Fracture of Engineering Materials & Structures*. **39**: 1319-1336.
15. Paolino DS, Tridello A, Chiandussi G, Rossetto M (2017) A general model for crack growth from initial defect in Very-High-Cycle Fatigue. *Procedia Structural Integrity*. **3**: 411-423.
16. Tanaka K, Akiniwa Y (2002) Fatigue crack propagation behaviour derived from S-N data in very high cycle regime. *Fatigue and Fracture of Engineering Materials and Structures*. **25**: 775-784.
17. Marines-Garcia I, Paris PC, Tada H, Bathias C, Lados D (2008) Fatigue crack growth from small to large cracks on very high cycle fatigue with fish-eye failures. *Engineering Fracture Mechanics*. **75**: 1657-1665.
18. Su H, Liu X, Sun C, Hong Y (2017) Nanograin layer formation at crack initiation region for very-high-cycle fatigue of a Ti-6Al-4V alloy. *Fatigue & Fracture of Engineering Materials & Structures*. **40**: 979-993.
19. Donahue RJ, Clark HM, Atanmo P, Kumble R, McEvily AJ (1972) Crack opening displacement and rate of fatigue crack growth. *International Journal of Fracture Mechanics*. **8**: 209-219.
20. Hong Y, Lei Z, Sun C, Zhao A (2014) Propensies of crack interior initiation and early growth for very-high-cycle fatigue of high strength steels. *International Journal of Fatigue*. **58**: 144-151.

21. Beretta S, Carboni M (2006) Experiments and stochastic model for propagation lifetime of railway axles. *Engineering Fracture Mechanics*. **73**: 2627-2641.
22. Paolino DS, Cavatorta MP (2013) Sigmoidal crack growth rate curve: statistical modelling and applications. *Fatigue & Fracture of Engineering Materials & Structures*. **36**: 316-326.
23. Kaplan EL, Meier P (1958) Nonparametric Estimation from Incomplete Observations. *Journal of the American Statistical Association*. **53**: 457-481.
24. Paolino DS, Tridello A, Chiandussi G, Rossetto M (2014) On specimen design for size effect evaluation in ultrasonic gigacycle fatigue testing. *Fatigue & Fracture of Engineering Materials & Structures*. **37**: 570-579.
25. Tridello A, Paolino DS, Chiandussi G, Rossetto M (2015) VHCF Response of AISI H13 Steel: Assessment of Size Effects through Gaussian Specimens. *Procedia Engineering*, 121-127.
26. Tridello A, Paolino DS, Chiandussi G, Rossetto M (2016) Different inclusion contents in H13 steel: Effects on VHCF response of Gaussian specimens. *Key Engineering Materials*, 49-52.
27. Li W, Sakai T, Li Q, Lu LT, Wang P (2010) Reliability evaluation on very high cycle fatigue property of GCr15 bearing steel. *International Journal of Fatigue*. **32**: 1096-1107.
28. Liu YB, Yang ZG, Li YD, et al. (2008) On the formation of GBF of high-strength steels in the very high cycle fatigue regime. *Materials Science and Engineering A*. **497**: 408-415.
29. Furuya Y (2011) Notable size effects on very high cycle fatigue properties of high-strength steel. *Materials Science and Engineering A*. **528**: 5234-5240.
30. Schuller R, Fitzka M, Irrasch D, Tran D, Pennings B, Mayer H (2015) VHCF properties of nitrided 18Ni maraging steel thin sheets with different Co and Ti content. *Fatigue and Fracture of Engineering Materials and Structures*. **38**: 518-527.
31. Paolino DS, Chiandussi G, Rossetto M (2013) A unified statistical model for S-N fatigue curves: probabilistic definition. *Fatigue & Fracture of Engineering Materials & Structures*. **36**: 187-201.
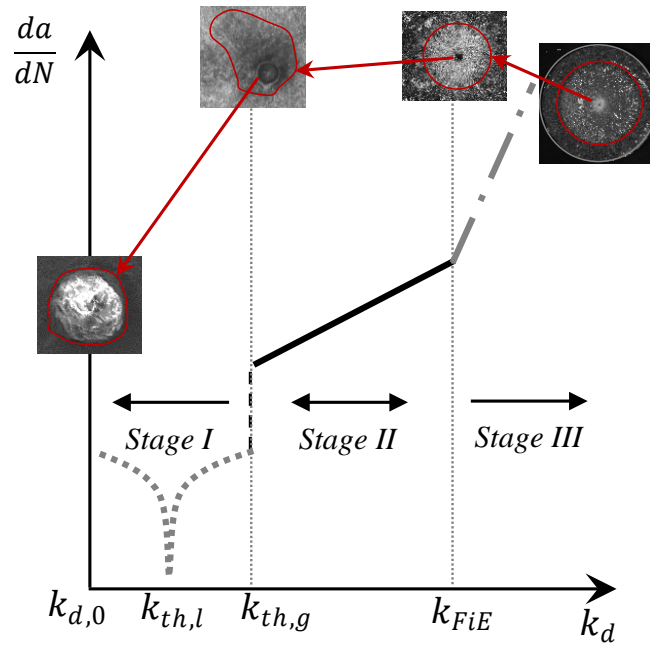
Figure 1: The three stages of crack propagation in a crack growth rate diagram for VHCF failures from internal defects.
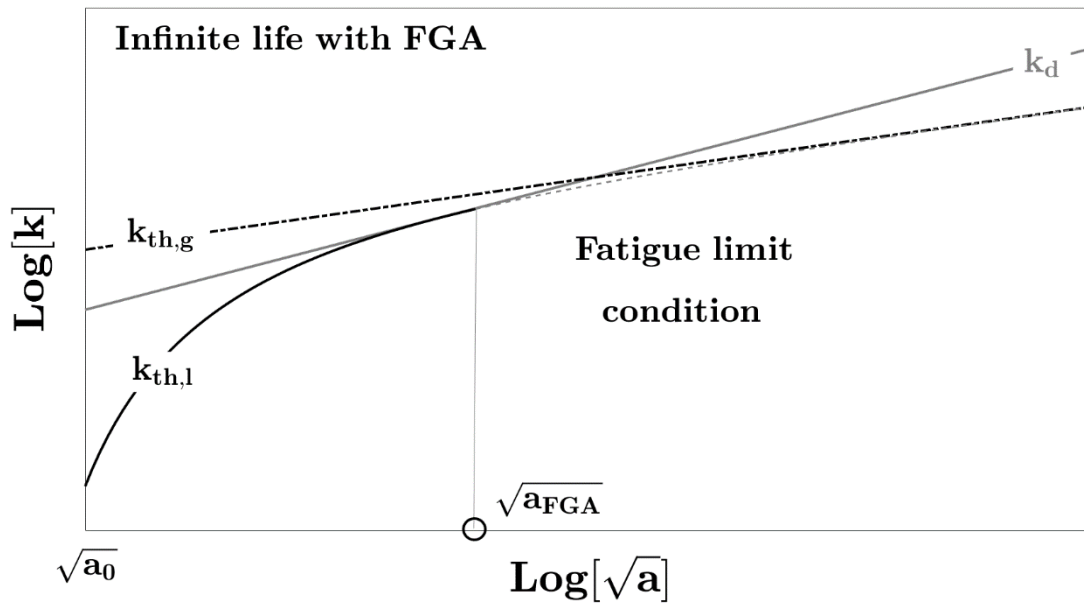

Figure 2: Variation of relevant SIFs with defect size in fatigue limit condition.
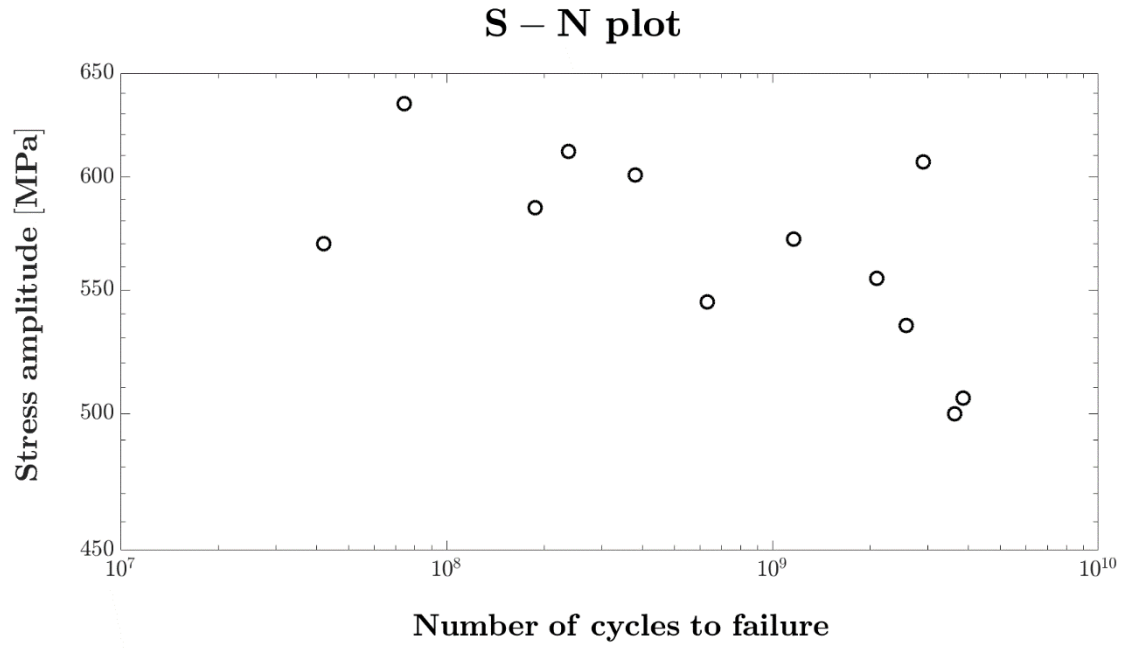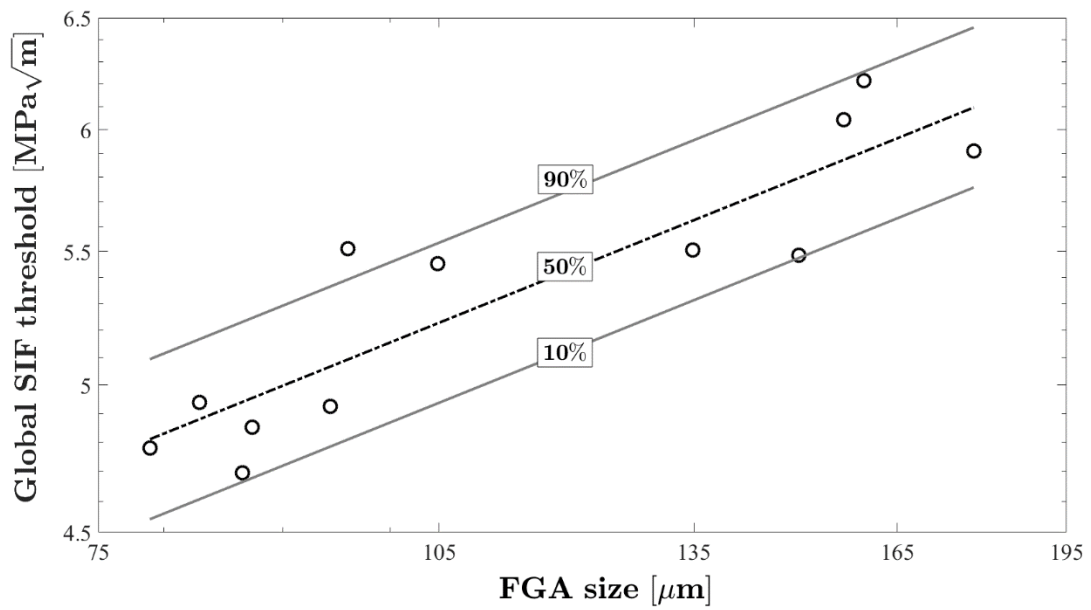
Figure 3: S-N plot of the experimental dataset.

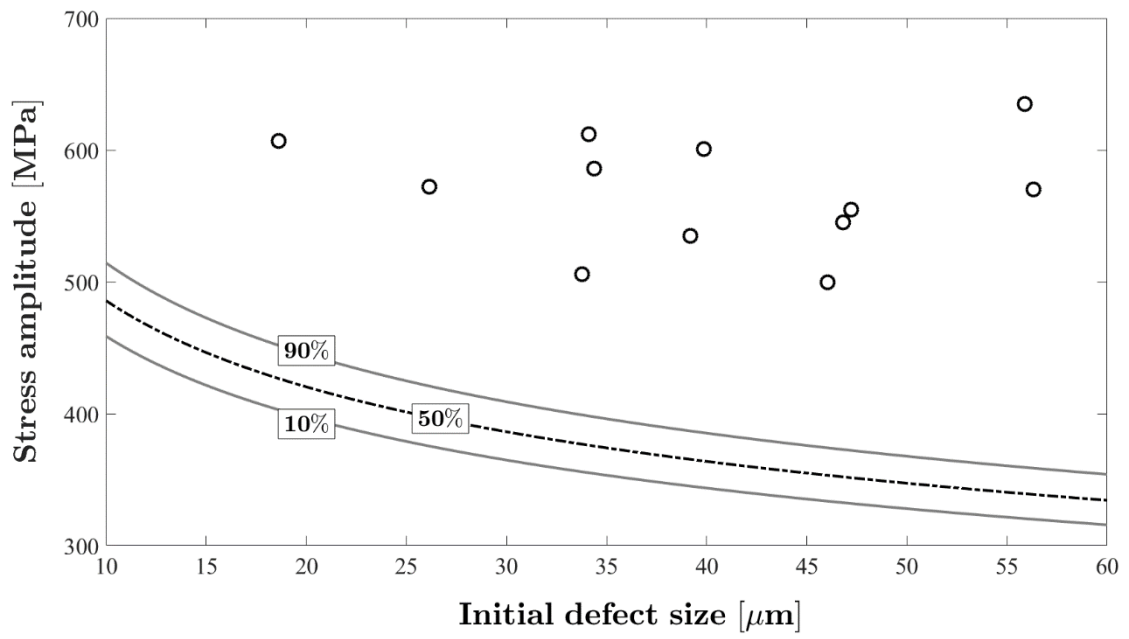Figure 4: Global SIF threshold variation as a function of the FGA size.

Figure 5: Variation of the fatigue limit with the initial defect size.
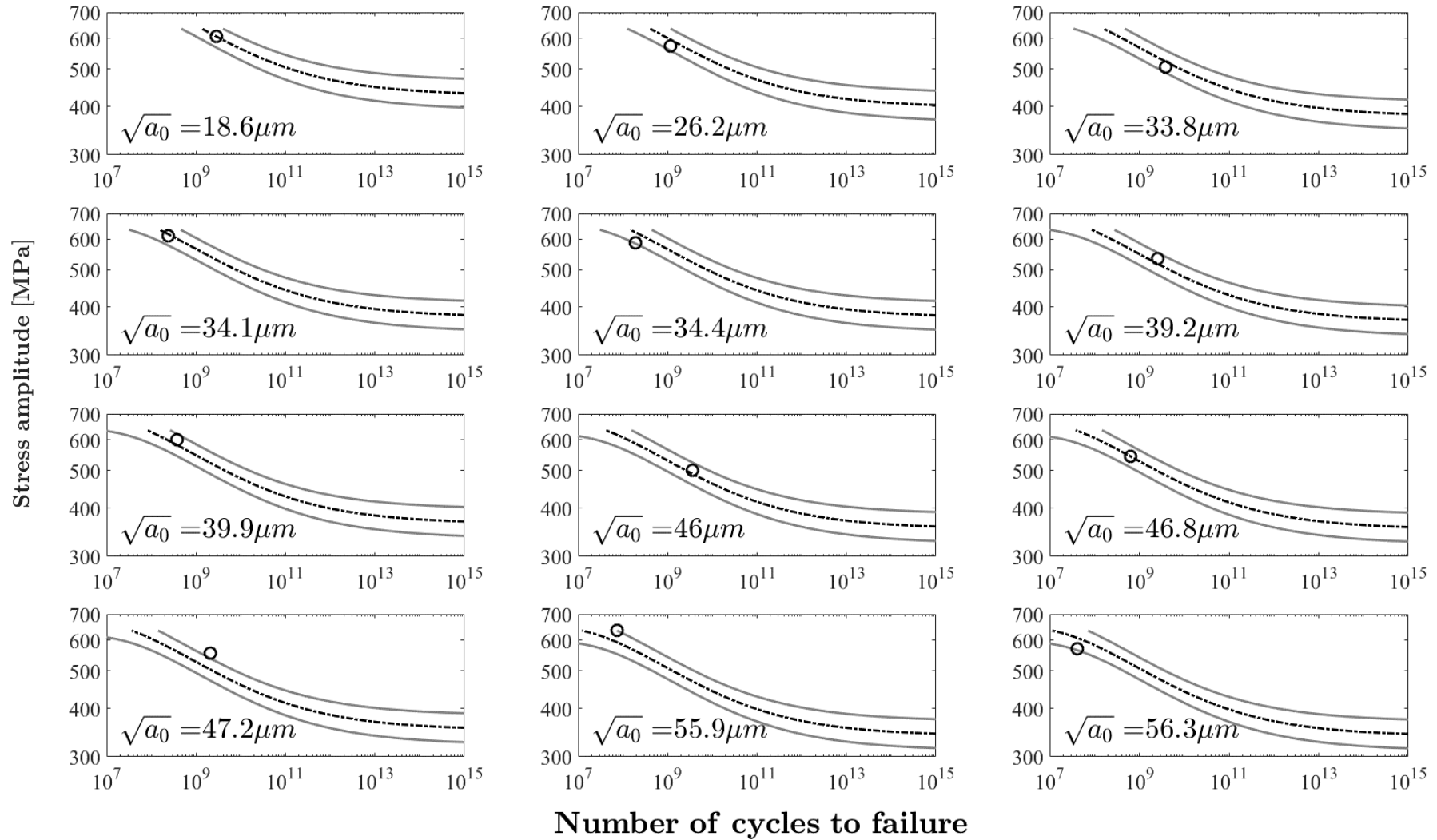
Figure 6: Conditional P-S-N curves estimated for the initial defect sizes of the experimental dataset. The three curves in each graph correspond to the 0.025-th, 0.5-th and 0.975-th quantiles of the VHCF life.
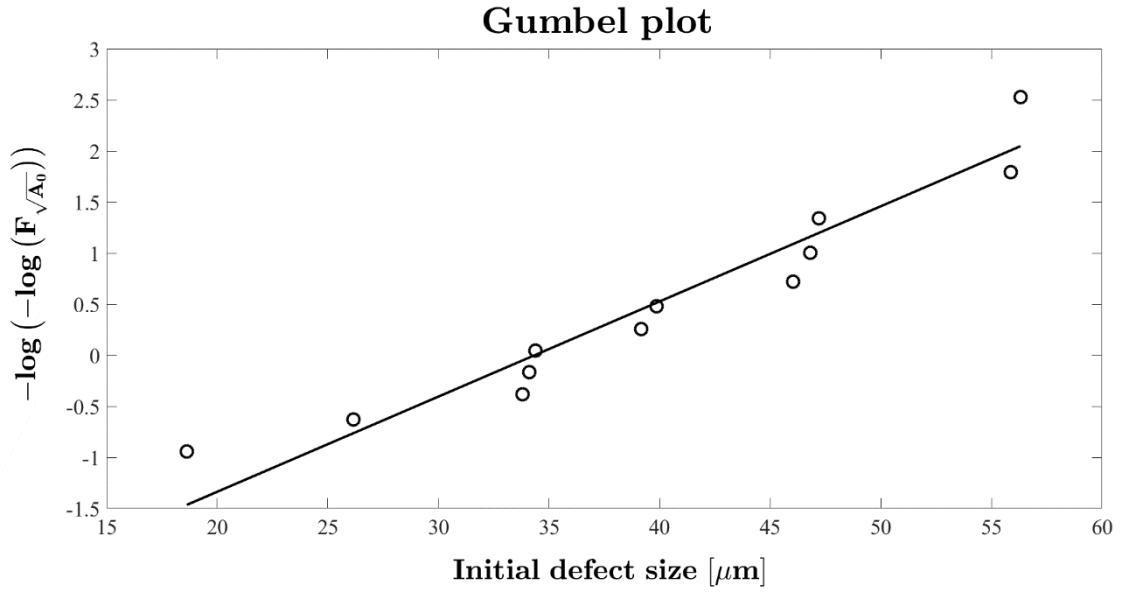
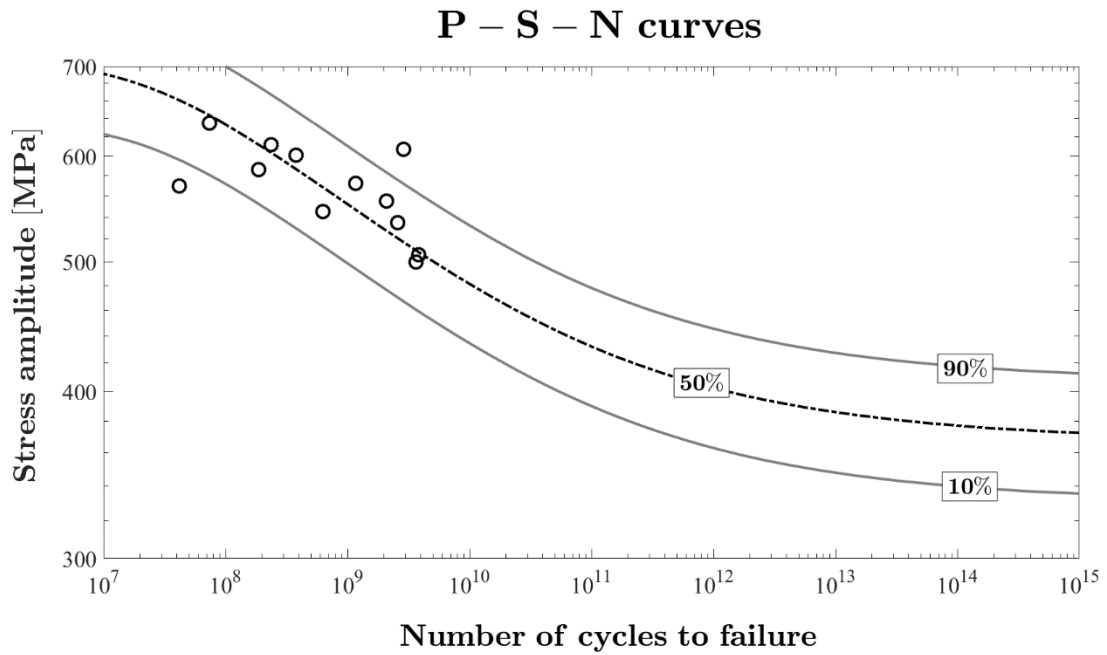Figure 7: Gumbel plot of the initial defect size for the investigated H13 steel.

Figure 8: Marginal P-S-N curves for the experimental dataset.